Int J CARS
DOI 10.1007/s11548-017-1583-8

ORIGINAL ARTICLE

Blood flow-induced physically based guidewire simulation for vascular intervention training

Jiayin Cai[1] · **Hongzhi Xie**[2] · **Shuyang Zhang**[2] · **Lixu Gu**[1]

Received: 23 September 2016 / Accepted: 30 March 2017

Abstract
Purpose A realistic guidewire behavior simulation is a vital component of a virtual vascular intervention system. Such systems are a safe, low-cost means of establishing a training environment to help inexperienced surgeons develop their intervention skills. Previous attempts to simulate the complex movement of a guidewire inside blood vessels have rarely considered the influence of blood flow. In this paper, we address this problem by integrating blood flow analysis and propose a novel guidewire simulation model.
Methods The blood flow distribution inside the arterial vasculature was computed by separating the vascular model into discrete cylindrical vessels and modeling the flow in each vessel according to Poiseuille Law. The blood flow computation was then integrated into a robust Kirchhoff elastic model. With hardware acceleration, the guidewire simulation can be run in real time. To evaluate the simulation, an experimental environment with a 3D-printed vascular phantom and an electromagnetic tracking system was set up, with clinically used guidewire sensors applied to trace its motion as the standard for comparison.
Results The virtual guidewire motion trace was assessed by comparing it to the comparison standard. The root-mean-square (RMS) value of the newly proposed guidewire model was 2.14 mm ± 1.24 mm, lower than the value of 4.81 mm ± 3.80 mm for the previous Kirchhoff model, while maintaining a computation speed of at least 30 fps.
Conclusion The experimental results revealed that the blood flow-induced model exhibits better performance and physical credibility with a lower and more stable RMS error than the previous Kirchhoff model.

Keywords Poiseuille Law · Blood flow analysis · Physically based guidewire simulation · Vascular intervention

Introduction

Cardiovascular disease is one of the most common causes of death [1] and is generally treated with medical management and minimally invasive vascular intervention surgery. As an alternative to heart medication, intervention surgery is widely performed throughout the world with the advantages of smaller incisions, less blood loss, decreased pain and quicker recovery [2]. Percutaneous coronary intervention (PCI) is an effective procedure used to treat stenotic coronary arteries in coronary heart disease. In this procedure, surgeons must manipulate a guide wire within a three-dimensional (3D) field while viewing its position on a two-dimensional screen [3]. Establishing a safe and low-cost training environment for inexperienced medical interns or students to master skills quickly is a challenging task. Traditional options, including synthetic phantoms, animals and human cadavers, are helpful but are subject to limitations [4,5]. The continuous development of virtual reality (VR) technology provides new possibilities for training. A VR-based simulation system provides a better means of training in an intervention procedure due to its more realistic views, higher flexibility, and easier training assessment [4]. Numerous studies have demonstrated that training using virtual reality simulation can improve inexperienced surgeons'

✉ Hongzhi Xie
drxiehz@163.com

✉ Lixu Gu
gulixu@sjtu.edu.cn

[1] School of Biomedical Engineering, Shanghai Jiao Tong University, Shanghai, China

[2] Department of Cardiology, Peking Union Medical College Hospital, Peking 100005, China

Published online: 09 April 2017

intervention skills [3,5,6]. The simulator can significantly decrease the time taken for the procedure, the amount of contrast fluid and the total fluoroscopy time [3].

A good guidewire movement model in a complex vascular structure simulation is a key component of a virtual vascular intervention simulation system. Tremendous work has focused on simulating a guidewire physically. In 2002, Lenoir et al. [7] proposed a dynamic one-dimensional Lagrangian splines model to simulate a wire-like structure in interactive time. This model provided a realistic bending effect but was limited by its inability to present a twisting effect. A new approach combining a real-time finite-element model with an optimization strategy based on substructure decomposition [8] permitted the representation of the complex behavior of wire-like surgical equipment in an effective manner, and a computer-based training system focusing on intervention was developed employing that method [9]. The substructure decomposition method avoided resolving the global stiffness matrix, allowing the computational time of FEM to be significantly reduced to real time, but motion errors were also propagated incrementally during the optimization. To overcome the shortcomings of substructure decomposition, an improved method computing the whole stiffness matrix and using the band structure of the matrix to inverse it [10] was proposed. Another model based on the principle of energy minimization [11] with several different optimization techniques displayed good performance in both the accuracy and stability of the simulation but was unsatisfactory for real-time interaction, even though acceleration methods were used.

Other researchers prefer modeling the guidewire as a discrete elastic rod such as mass spring model and Cosserat elastic rod model. Building on the Cosserat theory of elastic rods, Teschner [12] and Duratti et al. [13] implemented their simulation of a wire-like structure, which performed much better than the simple mass spring model [14,15]. Another work based on Cosserat theory [16] validated their simulation by comparing the position of a guidewire deployed in a vascular phantom with that of the simulated guidewire. Bergou et al. [17] proposed a Kirchhoff rods model, based on which Tang et al. [18] built a simulation system, solving the model with an implicit time integration method and dealing with collision using an Axis Aligned Bounding Box tree (AABB tree). However, the path of the guidewire in Tang's system was pre-planned and fixed, consequently making it not appropriate for training guidewire manipulation skills. Luo et al. [19] built an intervention simulator based on the Kirchhoff elastic rod model with an adaptive sampling method and k-dop tree for dealing with collision. This simulator showed good robustness and real-time performance, and the simulated guidewire was capable of entering the complex vascular structure without a pre-planned routine. However, none of these studies considered the force of blood on the guidewire when simulating guidewire movement in blood vessels.

Blood flow analysis and simulation are also popular topics. Alemder [20] presented a hydrodynamic model of human arterial blood flow and implemented his model with the C++ programming language as a cross-platform blood flow-simulating program. However, his model was too complex for individual adaptions based on patient-specific data. Based on Poiseuille Law and the Advection–Diffusion Model from the Navier–Stokes equations, Wu et al. [21] computed the blood flow in the common carotid artery and simulated the propagation of contrast agent in real time. Using a similar approach, Zhu et al. [22] built a sketch-based dynamic illustration system for fluids that is both easy and flexible for users to illustrate fluid systems not only in physiology but also in many aspects of engineering. Boisvert et al. [23] integrated blood circulation and a bleeding model into a computerized surgical simulation system by modeling the vessels as a graph and calculating the blood pressures and flows in real time. Pop et al. [24] visualized blood flow in a complex network in a direct particle system with the idea of layers of concentric tubes, and their particle system was also compatible with the Poiseuille Law.

The present paper, encouraged by Luo's [19] work on guidewire simulation using the Kirchhoff elastic rod method, sought to integrate blood flow computation to build a novel guidewire simulation model. The model was tested in the main artery corresponding to one of the PCI procedures that delivering the guidewire to the mouth of coronary artery. The continuous vascular model of the main artery is discretized into a series of cylindrical pipes, and the blood flow is analyzed using Poiseuille Law in real time. The resultant blood pressure and flow rate distribution are then integrated into the Kirchhoff model, and a simulated guidewire influenced by blood flow is proposed. As noted above, most researchers have not validated their results quantitatively. Tang et al. [16] did validate their work, but the position of the guidewire deployed in the phantom was computed based on images acquired using two identical cameras. To better validate the result of the proposed model, we introduce an electromagnetic tracking (EMT) system that can record the trace of the guidewire accurately to 0.6 mm, allowing the proposed virtual guidewire model to be compared with the real tracked guidewire in a 3D-printed vascular phantom.

Real-time blood flow computation

Flow model

The physical process of blood flowing through a complex vascular structure is difficult to describe due to the complexity of the flow model. However, as shown in Fig. 1, the blood

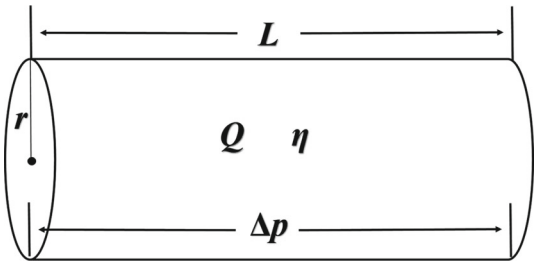

Fig. 1 A cylindrical pipe-like vessel

flow in a cylindrical vessel can be modeled with Poiseuille Law according to Eq. (1) [21], which is calculated from the Navier–Stokes equation to describe the laminar flow through a cylindrical pipe for an incompressible and Newtonian fluid

$$Q = \frac{\Delta p}{R} \quad \text{with } R = \frac{8\eta L}{\pi r^4}. \tag{1}$$

This equation models the blood flow in each part of the vessel as an incompressible viscous fluid flowing through a cylindrical pipe. It shows the relationship among the vessel flow rate Q, the pressure drop Δp in the vessel, blood viscosity η, vessel radius r and vessel length L.

Blood flow computation in vascular structure

The simulation in this paper focuses on a guidewire moving inside the main artery. As Poiseuille Law is for smooth, straight tubes but the structure of the main artery is complex, a bunch of cylindrical pipes was used to approximate the original model. As shown in Fig. 2, the original vascular model (a) generated from medical imaging data is divided into cylindrical pipes (c) based on the centerline (b). A library named VMTK [25] is used to compute the centerline. Based on the extracted centerline, the continuous vascular structure is separated into cylindrical vessels, the combination of which is an approximation of the original structure. The blood flow in each cylindrical vessel thus becomes appropriate for Poiseuille Law modeling as in Eq. (1).

Then, the separate vessels in the discrete vascular structure are connected and can be represented as a directed graph [21] $G(N_\mathrm{n}, N_\mathrm{e})$, with N_n nodes and N_e edges. Each node represents a separate point, and each edge represents a cylindrical vessel. A node–edge adjacency matrix A is introduced to describe the topological structure of the graph, which has N_n rows and N_e columns. For each element in A,

$$A_{i,j} = \begin{cases} 1 & \text{if edge } j \text{ starts from node } i \\ -1 & \text{if edge } j \text{ end in node } i \\ 0 & \text{otherwise.} \end{cases} \tag{2}$$

A set of equations can be developed as follows.

Except the leaf nodes, which have no edge to start from, the blood entering and leaving each node is always at the same level. With the node–edge adjacency matrix, this relation can be expressed as the following equation:

$$AQ = 0. \tag{3}$$

For all edges in the graph, the Poiseuille Law can be represented in matrix form as

$$CQ = \Delta P \tag{4}$$

where C is a diagonal matrix of $\begin{pmatrix} R_1 & \dots & 0 \\ \vdots & \ddots & \vdots \\ 0 & \dots & R_{n_\mathrm{e}} \end{pmatrix}$ and ΔP is a vector containing the pressure drop of all edges.

The blood flow is driven by a periodical external pressure source from the heart. A time-varying pressure source is then added to the root node of the graph to force the blood to flow through the vessels. The pressure source can be modeled as a sinusoidal function [23] that varies with time, changing between systolic pressure P_1 and diastolic pressure P_2:

$$p_\mathrm{source}(t) = \frac{P_1 - P_2}{2} \sin(\omega t) + \frac{P_1 + P_2}{2}. \tag{5}$$

Combining Eqs. (1) through (5), the blood flow in the whole vascular structure can be solved by the following matrix form equation:

$$\begin{pmatrix} A & 0 \\ C & A^\mathrm{T} \end{pmatrix} \begin{pmatrix} Q \\ P \end{pmatrix} = \begin{pmatrix} 0 \\ P_\mathrm{source}(t) \end{pmatrix} \tag{6}$$

where Q denotes the vector containing the flow rate in each cylindrical vessel, P refers to the vector of pressure value in each node of the separate vascular model, and $P_\mathrm{source}(t)$ is deduced from (5).

The equation can be solved explicitly as shown in Eq. (7):

$$\begin{pmatrix} Q \\ P \end{pmatrix} = K^{-1} \begin{pmatrix} 0 \\ p_\mathrm{source}(t) \end{pmatrix} \quad \text{with } K = \begin{pmatrix} A & 0 \\ C & A^\mathrm{T} \end{pmatrix}. \tag{7}$$

The vascular structure is fixed after it is loaded and K is invariant; thus, K^{-1} can be pre-computed, which leads to less variability in time and less expense on hardware resources during the simulation and permits real-time computation rates even for a complex structure.

Moreover, the pressure values across the cylindrical vessels are linearly interpolated based on the pressure values at their starting and end points, which are computed in advance using the equation sets described above.

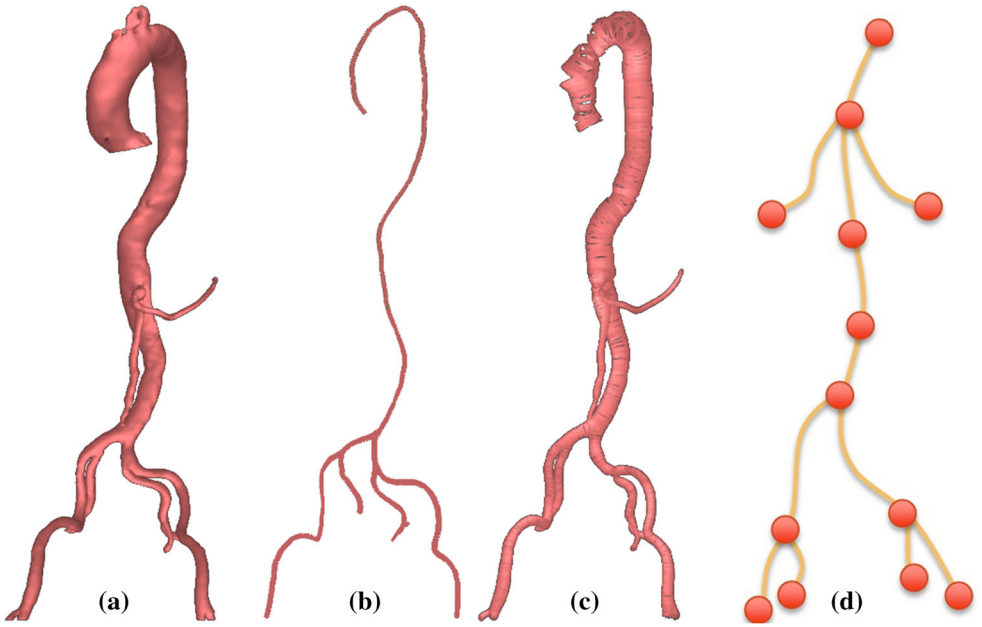

Fig. 2 Discretization of the vascular model. **a** Original model, **b** centerline, **c** discrete model, **d** abstract model as a directed graph

Blood flow-induced guidewire simulation

Based on Luo's Kirchhoff elastic rod approach [19], guidewire movement in the vascular model is simulated. To consider blood flow, each mass point of the simulated guidewire must be located in the separate vascular model, i.e., the cylindrical vessel that the mass point is in must be determined. It is never wrong to check the relative position of each mass point in each vessel when the mass point must be located in the closest vessel; however, the quadratic complexity of this task means that it can take dramatically longer to complete, especially given hundreds of thousands of vessels and mass points of the guidewire. Our strategy is based on the observation that a series of neighboring mass points usually remain in roughly the same or neighboring vessels. Therefore, if we represent all mass points as $m_{1\sim n}$ and all vessels as $V_{1\sim n}$, it is only necessary to search each vessel from V_1 to V_n for the first mass point m_1 and find the relative vessel $V_{1'}$. For the other points m_i, we search the vessels $V_{(i-1)'\pm a}$, which is only a small neighborhood with length $2a$ that mass point m_{i-1} is located in.

After we locate each mass point m_i in a vessel $V_{i'}$, we can define the influence of the blood flow on each mass point. From the vessel flow rate Q and the pressure drops ΔP computed by the vascular flow model described above, the laminar flow velocity along the axial direction of each vessel is modeled as Eq. 8:

$$u(x,d) = \frac{1}{4\eta}\frac{\Delta P}{x}\left(r^2 - d^2\right) = \frac{2}{\pi r^2}Q\left(1 - \frac{d^2}{r^2}\right) \tag{8}$$

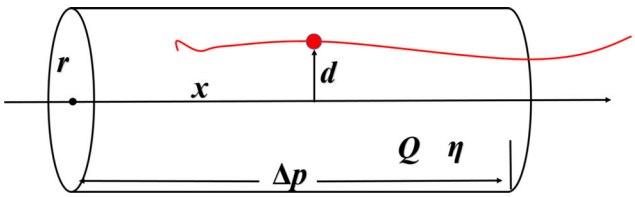

Fig. 3 Guidewire moving in a vessel modeled with the flow equation

which indicates the laminar flow velocity at any position in a vessel varying with the radical direction distance d and the axial direction distance x [21].

Figure 3 shows a guidewire entering a vessel filled with blood flow. According to the location of each mass point in the vessels and Eq. 8, the flow velocity at every mass point can be computed and integrated into Luo's [19] guidewire model. The dynamic iteration of Luo's [19] original guidewire model is expressed in Eq. 9, where x_t and v_t are the location and velocity at time t with the variation of locations (Δx) and velocity (Δv), respectively, in time step Δt. M is a diagonal mass matrix associated with the mass point positions, and $\partial f/\partial x$, $\partial f/\partial v$ are the Jacobian matrices of the force with respect to locations and velocities. With the flow velocity u computed from Eq. 8 as an additional item in Eq. 10, the guide wire simulation is now under the influence of blood flow.

$$\begin{bmatrix}\Delta x\\ \Delta v\end{bmatrix} = \Delta t\begin{bmatrix}v_t + \Delta v\\ M^{-1}f\left(x_t + \Delta x, v_t + \Delta v\right)\end{bmatrix} \tag{9}$$
$$f\left(x_t + \Delta x, v_t + \Delta v\right) = f_t + \frac{\partial f}{\partial x}\Delta x + \frac{\partial f}{\partial x}\Delta v$$

$$\begin{bmatrix} \Delta x \\ \Delta v \end{bmatrix} = \Delta t \begin{bmatrix} v_t + \Delta v \\ M^{-1} f\,(x_t + \Delta x, v_t + \Delta v) \end{bmatrix} + \begin{bmatrix} 0 \\ u \end{bmatrix}. \tag{10}$$

Experiments and evaluation

In the experiment, the blood flow was first computed in a vascular model. A visualization was created that included the flow rate and pressure distribution. The influence of flow was then applied to the mass points of the simulated guidewire to find the difference between simulations with and without the influence of blood flow. With the aid of an EMT system, we also compared the computer-generated guidewire movement with that of a real guidewire deployed in a 3D-printed phantom. The simulation system was developed and tested on a PC with Intel® Xeon® E3-1230 CPU, 4G memory and an NVidia GeForce GTX 760 GPU.

Flow computation result

The vascular model was the main artery generated from a patient's CT scan, which was segmented according to a semiautomatic algorithm [26]. Before the blood flow computation, the centerline of the model was extracted with the aid of the VMTK library and the model was separated into discrete vessels. The discrete vascular structure, including 2477 vessels, was modeled as a directed graph with 2478 nodes and 2488 edges. The Intel MKL library was used to pre-compute the inverse of matrix K and perform the matrix multiplication during the simulation. Approximately 9 milliseconds per frame was required to compute the distribution of blood pressure in the vascular model.

The computation result is illustrated in Fig. 4a, where higher pressure is represented as red and lower pressure as blue. Figure 4b shows that the pressure varies with the vessel radius. The pressure decreases significantly when the vessel radius decreases, consistent with Poiseuille Law—the pressure drop ΔP in a cylindrical vessel is inversely proportional to the 4th power of the radius (r^4).

FEM computation was introduced to evaluate our flow results. Due to the limitations of current meshing techniques and the PC hardware, it is impractical to compute flow over the whole vascular model with FEM. Instead, a small section with a branch structure was derived from the vascular

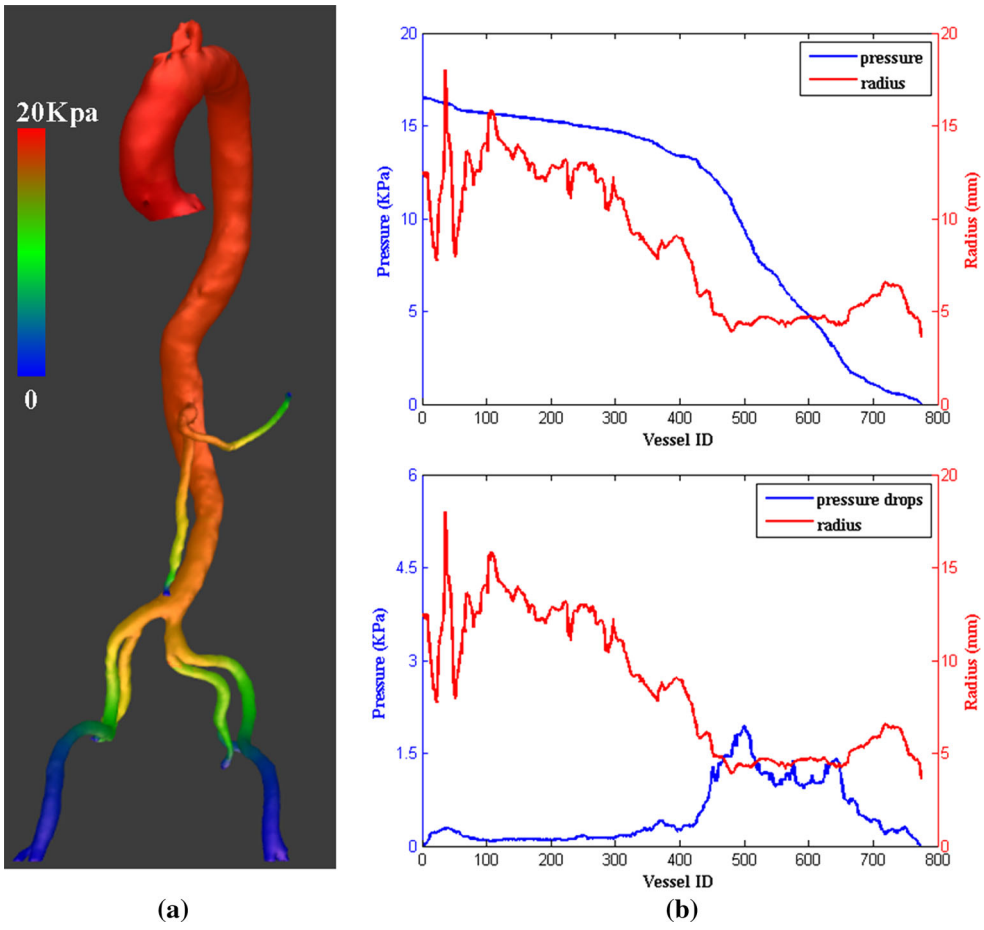

Fig. 4 **a** Blood pressure distribution in the vascular model, **b** pressure and pressure drops corresponding to the vessel radius

Table 1 Comparison of the pressure values (KPa) of the model and the FEM results

Sampling	#1	#2	#3	#4	#5	#6	#7	#8	#9	#10
Our model	12.85	12.78	12.32	11.51	10.40	10.20	9.92	9.60	9.27	9.05
FEM	12.85	12.58	12.15	11.52	12.15	10.37	10.26	10.50	9.42	9.05

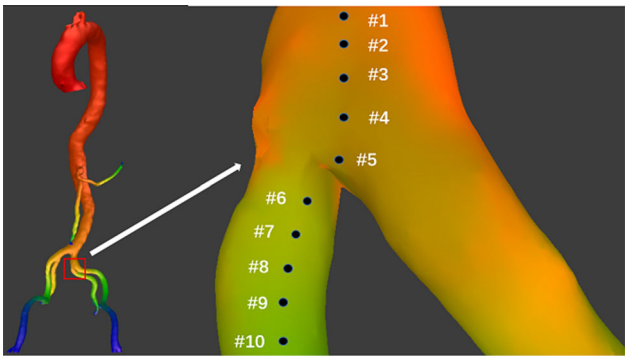

Fig. 5 Sampling points on the model surface

model and FEM was applied with the same boundary conditions. The comparison of 10 sampling points on the surface of the model is presented in Table 1. As shown in Fig. 5, the sampling points are located along the flow direction, and 5 points after #6 are located in one of the branches. Under the same boundary condition, the pressure values of both our model and the FEM results exhibit a descending trend, but the FEM results present better local details, such as point #5 (a branching position) and point #8 (a bulge of the surface).

Comparison of simulating guidewire with/without blood influence

We performed a simulated intervention by driving the two simulated guidewires into the vascular model using a constant force with and without the influence of blood flow simultaneously. The simulation target was a "J"-tipped 0.035 wire, which is commonly used in PCI procedures. As shown in Fig. 6, four snapshots captured during the process show that the motion shape of the guidewire is more bent and closer to the vessel wall under the influence of blood flow (green) but remains straight without blood pressure (white). Figure 7a shows the distance from the entry of each mass point along the guidewire. Although the two guidewires are identical in terms of the total length, the proposed guidewire model creates a greater number of and more specific sampling mass points because of the blood flow effect and the adaptive sampling strategy [19]. Figure 7b shows the comparison of the force magnitude that each mass point bears, including collision and blood force.

Evaluation of the simulated guidewire with a real EMT tracing

Experiment setup

Figure 8 shows the hardware setup for the experiment. A vascular phantom was prepared with TangoPlus and VeroClear hybrid materials using an Object500 Connex3 3D-printing machine from Stratasys Company. The 3D-printed phantom was based on the same vascular model generated from patient CT scans in our simulated environment and printed with a thickness of 4 mm. For coordinate transform convenience, 4 additional landmarks were attached to the phantom and the phantom was fixed to a PVC board. The hybrid material we used is more stable, which ensures the shape consistency (alignment) of the phantom and the vascular model in establishing our simulation environment. Perhaps the elastic properties of the hybrid material are not very close to the elastic properties of an actual vascular system, however, as the elasticity of the vessel wall is not considered in our model, and the elastic property of the printed material is assumed to have a negligible effect on the movement of the guidewire.

The guidewire we inserted into the phantom was an EMERALD Guidewire 0.035 from Cordis Corporation and the same guidewire used clinically. As the tip status of guidewire motion is most crucial during surgery, 3 NDI Aurora 610058 5DOF magnetic sensors were bound to the tip of the guidewire to allow the NDI Aurora EMT system to provide the specific positions of the guidewire tips in the phantom during the experiment and tracking of the motion.

In the experiment, the phantom was placed in a transparent water tank filled with 10% aqueous glycerol adjacent to an EM field generator. An optical motion detector was used to synchronize the movement of the real guidewire in the 3D-printed phantom and the guidewire in the virtual environment. An external water source was generated to simulate the flow pressure source from the heartbeat.

Figure 9 shows the experimental procedure. After the setup and resources were loaded in the system, registration was performed through the landmarks to compute the transform relationship between the actual and simulated coordinate. We then deployed the real guidewire in the phantom, and the optical motion detector was used to drive the synchronous advancement of the virtual guidewire. The guidewire was inserted into the vascular model from the right low branch, consistent with the approach in real surgery.

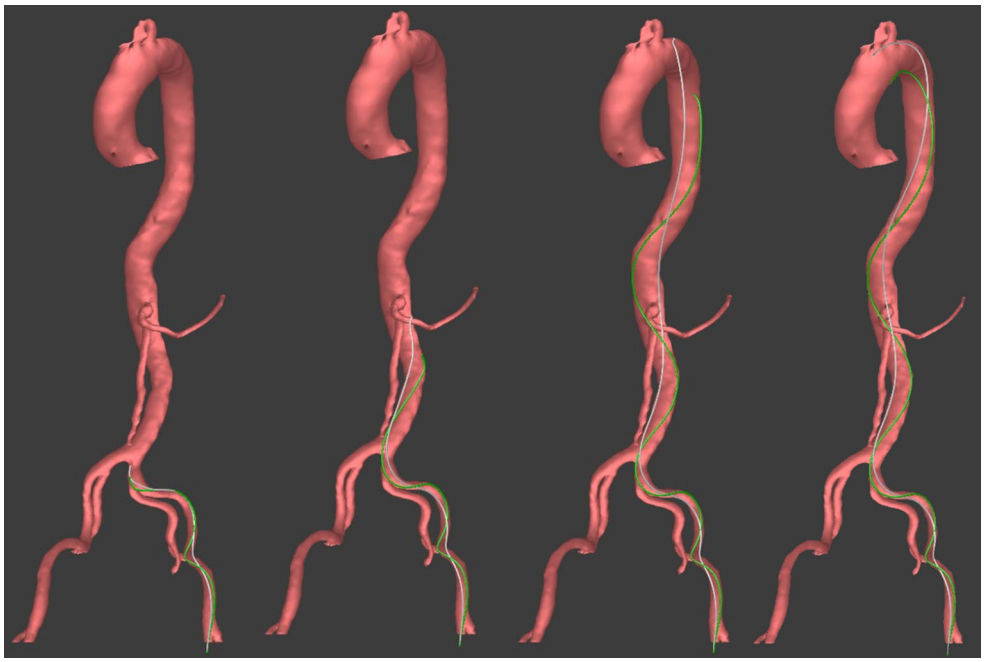

Fig. 6 Four snapshots of the comparison of simulating the guidewire with (*green*) and without (*white*) the influence of blood flow

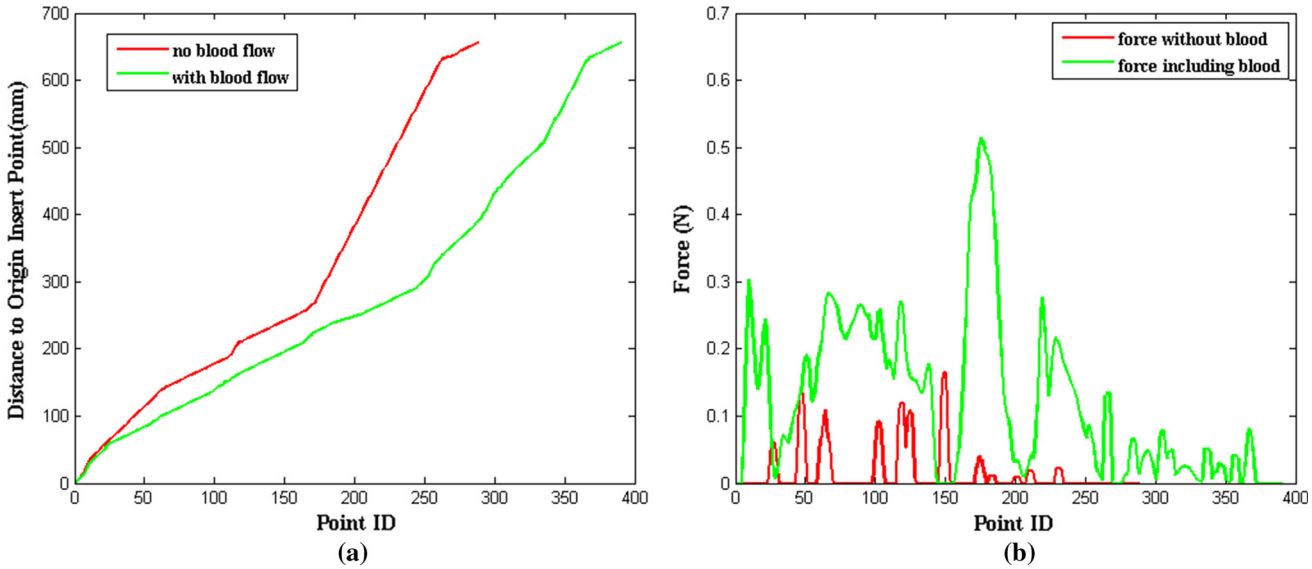

Fig. 7 Data analysis of the simulated guidewire. **a** The distance from the entry of each mass point along the wire, **b** the magnitude of force each mass point bears, including both collision and blood force

For validation purposes, the trace of the physical guidewire tip was recorded by the EMT system, and the simulated guidewire tip trace was also logged by the system. Both traces were recorded with a 5-mm sampling interval. The experiment was performed by inserting the guidewire into the phantom through different branches and at different speeds, with multiple times for each condition for reproducibility and to eliminate the chance of accidental coincidence.

Error measures

The physical guidewire tip trace recorded using the EMT system could be regarded as the true measure for evaluating the simulated tip traces. We used the root-mean-square (RMS) distance between the two traces to measure the result, computed as

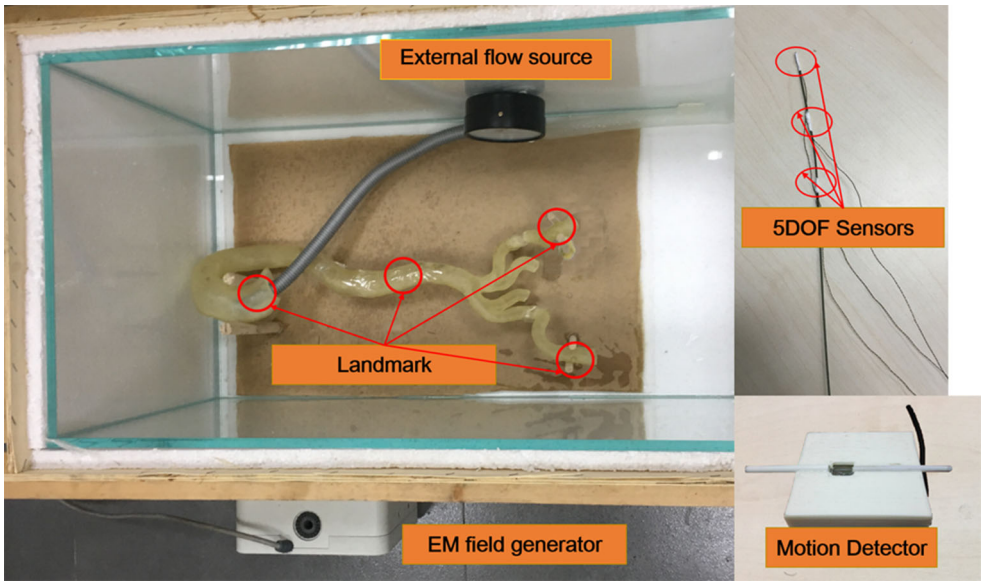

Fig. 8 Experimental hardware setup

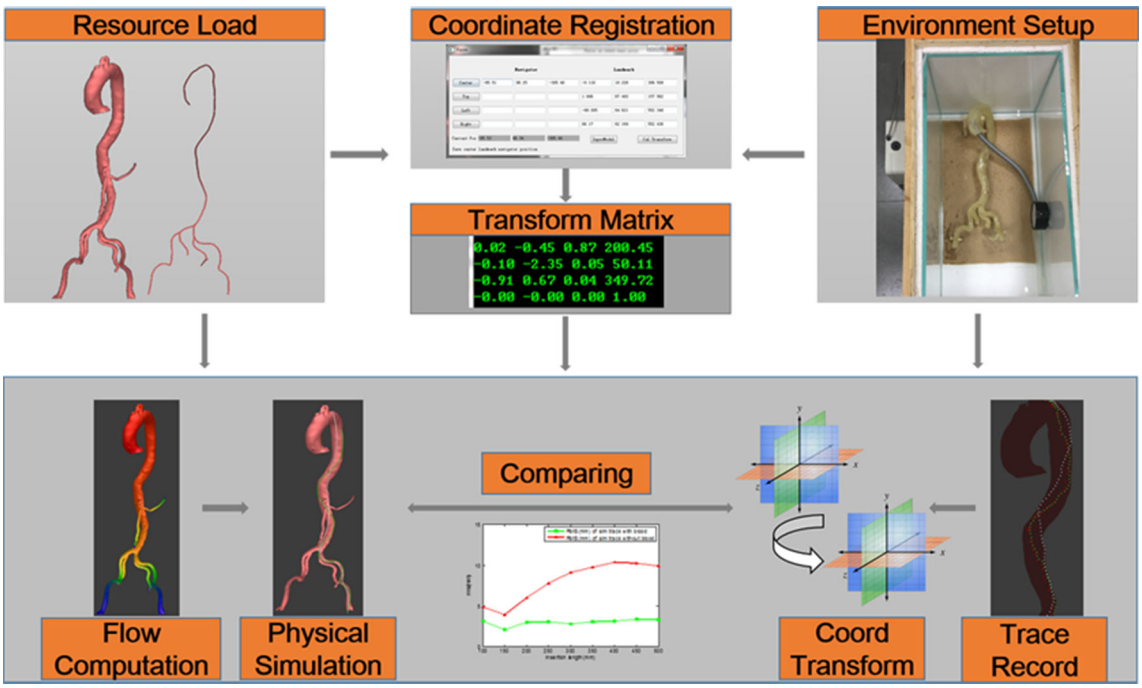

Fig. 9 Experimental procedure

$$\mathrm{RMS} = \left(\frac{1}{2}\sum_{1}^{n}(X_i - Y_i)^2\right)^{1/2} \tag{11}$$

where X denotes the n simulated trace points and Y denotes the corresponding reference positions of the physical trace.

Experimental results

Figure 10 presents 3 tip traces: the trace (blue) of the real guidewire in the phantom and the traces of the simulated guidewire with (green) and without (white) blood flow influence, including 2 groups of experimental results with the

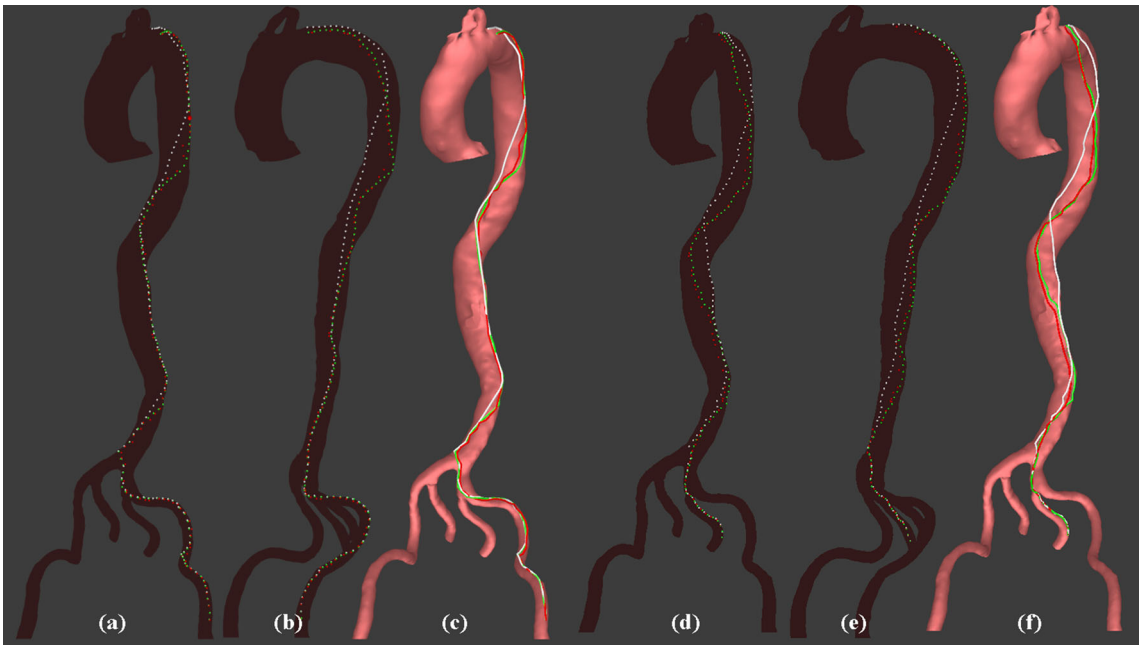

Fig. 10 Comparison of the simulated guidewire tip trace with the real guidewire tip trace recorded by the EMT system, visualized as the front view (**a**, **d**), side view (**b**, **e**) and view of connected isolated points (**c**, **f**). The *green trace* represents the model simulated with blood force; the *white trace* represents the model simulated without blood force; the *red trace* is the real trace recorded by the EMT system

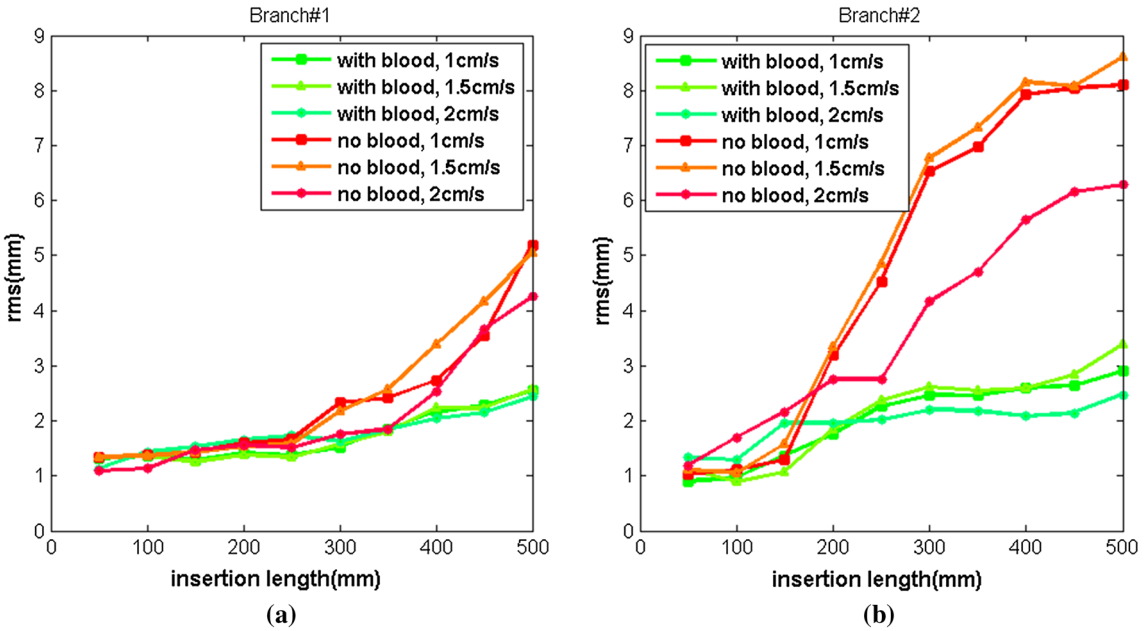

Fig. 11 Comparison of the virtual and EMT recorded traces of the guidewire inserted through branch #1 (**a**) and branch #2 (**b**) at different speeds. The *horizontal axis* denotes the insertion length, and the *vertical axis* denotes the RMS in millimeters

guidewire inserted through different branches (a, b, c from one group and d, e, f from the other). The trace of the simulated guidewire tip with flow influence more closely resembles the EMT real trace in both position and trend.

The quantitative comparison of the real and virtual traces is presented in Fig. 11 and Table 2, showing the experimental results of the guidewire inserted through branch #1 and branch #2 at 3 different speeds. Figure 11 shows the RMS value changes as the guidewire insertion length increases. The RMS of both simulated guidewire traces is initially small because the blood flow pressure is low in those areas due to the small vessel radius and long distance from the pressure source (heart). However, as the guidewire approaches the pressure source, the increasing flow pressure dramati-

Table 2 RMS of the real and virtual traces

Speed (cm/s)	Length	RMS (with blood)	RMS (no blood)	Length	RMS (with blood)	RMS (no blood)
Branch #1						
1	50	1.31	1.33	300	1.52	2.32
	100	1.37	1.37	350	1.85	2.42
	150	1.28	1.43	400	2.16	2.73
	200	1.41	1.59	450	2.29	3.55
	250	1.38	1.66	500	2.55	5.19
1.5	50	1.34	1.34	300	1.58	2.17
	100	1.37	1.36	350	1.80	2.57
	150	1.26	1.44	400	2.24	3.38
	200	1.38	1.53	450	2.23	4.16
	250	1.34	1.59	500	2.57	5.04
2	50	1.12	1.09	300	1.63	1.76
	100	1.43	1.13	350	1.84	1.86
	150	1.54	1.47	400	2.04	2.54
	200	1.66	1.55	450	2.15	3.67
	250	1.73	1.52	500	2.44	4.26
Branch #2						
1	50	0.90	1.02	300	2.47	6.52
	100	0.96	1.12	350	2.46	6.97
	150	1.36	1.30	400	2.60	7.92
	200	1.75	3.19	450	2.63	8.04
	250	2.27	4.53	500	2.90	8.10
1.5	50	1.13	1.11	300	2.61	6.78
	100	0.90	1.05	350	2.55	7.32
	150	1.08	1.59	400	2.59	8.15
	200	1.84	3.34	430	2.85	8.07
	250	2.38	4.86	500	3.39	8.61
2	50	1.34	1.19	300	2.20	4.17
	100	1.29	1.69	350	2.18	4.71
	150	1.97	2.17	400	2.08	5.65
	200	1.96	2.75	450	2.14	6.16
	250	2.02	2.76	500	2.47	6.29

cally affects the RMS. The blood flow influenced guidewire exhibits significantly improved performance, with a lower and more stable RMS of 2.14 mm $\pm$ 1.24 mm, less than half of the value of 4.81 mm $\pm$ 3.80 mm for the simulated guidewire without the influence of blood flow.

Efficiency evaluation

An acceptable simulation must be run in real time. Table 3 and Fig. 12 show the summary of the efficiency, including the time costs of flow computation, physical computation, collision handling, application of flow force and rendering. As the vascular structure is immutable and the inverse of the matrix K is pre-computed, the flow computation in each frame is nearly constant at approximately 9 ms. Other parts of the computation are of linear complexity with respect to the size of mass point size. The whole simulation procedure can run in 30 fps, which is faster than the real-time threshold of 24 fps.

Initial clinical tests

The proposed model was applied and integrated into our simulator for PCI training as shown in Fig. 13, which includes a software system for virtualizing the surgical procedures and a hardware system that provides related haptic feedback and a guidewire insertion interface [19].

Table 3 Computation time distribution (ms)

Mass point size	50	100	150	200	250	300	350	400
Flow computation	9.31	9.23	9.19	9.12	9.27	9.09	9.02	9.15
Collision handling	0.52	1.02	1.28	2.23	2.31	2.96	3.17	4.71
Physical computation	1.51	2.68	2.97	4.04	4.83	8.57	9.45	8.12
Adding flow force	0.66	0.77	1.08	1.36	1.70	2.02	2.28	2.63
Rendering	2.36	3.19	3.57	4.68	5.08	5.73	6.65	7.65
Total time	14.37	16.89	18.09	21.44	23.20	28.37	30.56	32.26

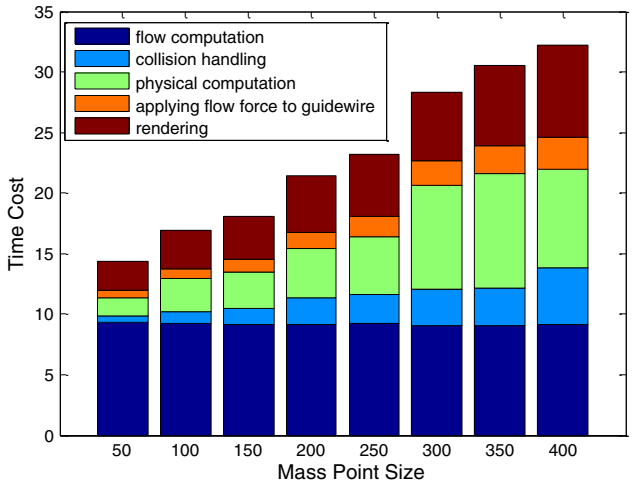

Fig. 12 Efficiency of each simulation step

To evaluate the simulator and the proposed model, an experiment was conducted in which three experienced interventionists were invited as group 1 and asked to perform the PCI procedure 10 times each while the guidewire was simulated with blood influence on and off. The operation time was recorded, and the times of fluoroscopy applied counted. As shown in Fig. 14, the mean performance was better in the blood flow influenced model, which presents a simulation more identical to the real situation in the experience of the interventionists.

Five medical students without any intervention experience were invited as group 2. The students had already observed the operations by group 1 and were asked to perform the intervention 20 times with the blood influence model. The performance was recorded and is plotted in Fig. 14. The mean performance of group 2 improved as the number of operation times increased. This is a good indication that the simulator is effective for interventional training, but a larger study is needed in order to obtain any statistical significance.

Discussion and conclusion

This paper presents a realistic simulated guidewire model by integrating blood flow computation into a previous Kirchhoff guidewire simulation model [19]. The simulation can be performed in real time with the aid of hardware acceleration, and the quantitative validation with the EMT system indicates a high level of physical fidelity.

In this paper, the vascular structure is abstracted into a direct graph, and in each unit, the Poiseuille Law is introduced to model the blood flow. The hardware acceleration cuts down the time cost of the flow computation to real time, and the flow analysis result is then applied to the guidewire based on the Kirchhoff elastic rod method, which provides a blood flow influenced virtual guidewire. The finite-element method is another option for flow computation and can provide a more accurate and detailed flow analysis. However, the meshing technique is very difficult for a multi-scale geometric model with complex structures such as the vascular model in our experiment, and it is a very professional job to smooth the vascular surface mesh that FEM requires. Based on the existing PC calculation ability, a long preparation time would be required to add a new patient-customized vascular model. The FEM benchmark test in this paper reveals that the FEM provides more details at specific regions, with discrepancies occurring only in local regions and with limited influence on the consistency of the flow distribution and trend over the whole vascular structure. The proposed method may be more flexible and general for a variety of applications than the FEM method.

To evaluate our simulation results, we also record the real trace of guidewire movement in a 3D-printed phantom using an EMT system. The comparison of the real and virtual guidewires indicated a high level of physical fidelity for the simulation performance. The RMS value was 2.14 mm $\pm$ 1.24 mm, which is not as good as the validation result in another research paper [16], perhaps because the previous authors only validated their simulated guidewire in small vessels such as coronary arteries with a diameter of up to 5 mm. Our evaluation was performed in far larger vessels of the main artery with diameters of up to 30 mm, which have more free space in which the guidewire can move and thus introduce more RMS into our validation. As shown in Fig. 11 and Table 2, the RMS value is comparable to the previous results when the guidewire is used in smaller vessels.

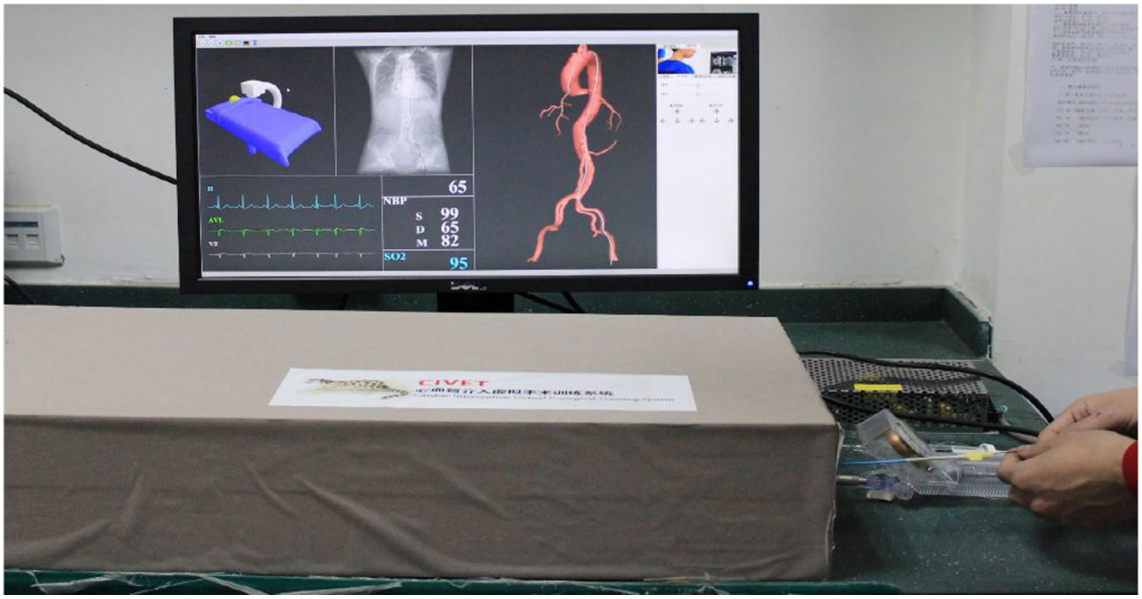

Fig. 13 Simulator for PCI training

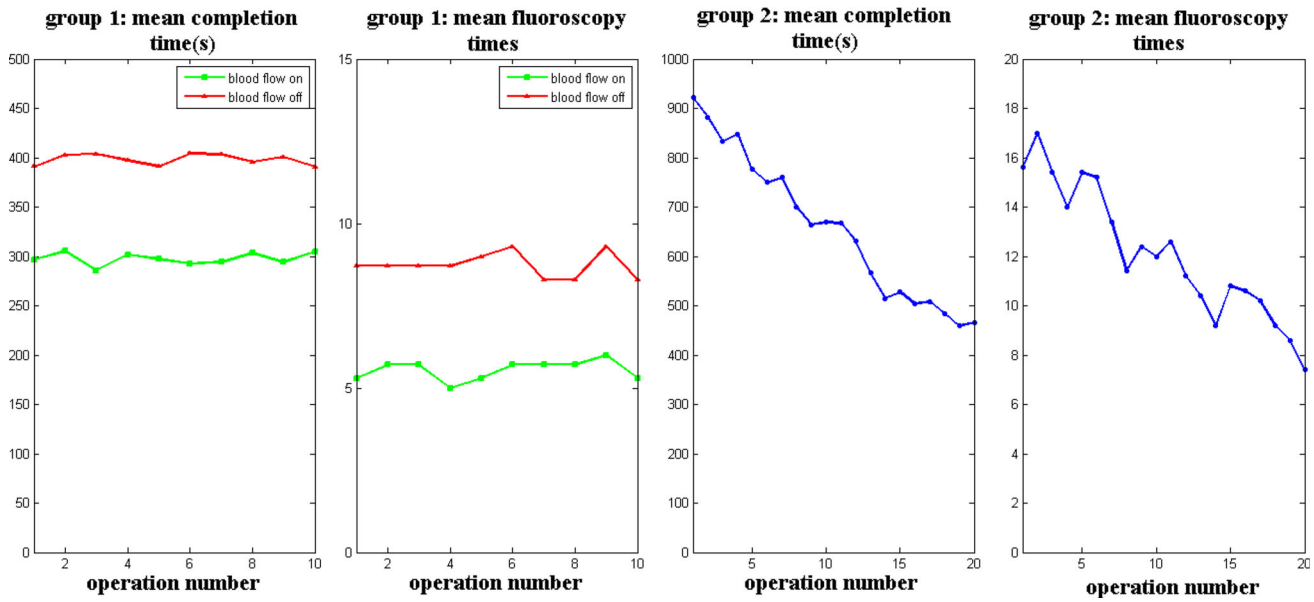

Fig. 14 Performance

The simulation result received positive comments from doctors due to its improved physical fidelity compared to the existing simulator based on the evaluation experiments. The doctors confirmed that improving guidewire simulation would be useful in helping trainees better understand the movement of the guidewire in the blood vessel and would more efficiently improve their intervention skills. Furthermore, as the pressure of the blood flow and the force of each simulated mass point bearing have already been computed, the proposed method holds potential to produce more specific haptic feedback in an interactive virtual reality training system for vascular intervention surgery and thus to contribute to establishing a more realistic training environment for trainees.

The flow model is based on an axially oriented laminar flow model, which is imperfect because it neglects other factors such as turbulent flow, the influence of systole and diastole on flow patterns, non-Newtonian fluid behavior and the elasticity of the artery wall. These factors could greatly increase the complexity of the simulation model and require much more computation time. The flow model presented in this paper represents a balance of physical fidelity and real-

time computation under the current experimental conditions, but those factors are points requiring further research and consideration in our future work.

Acknowledgements This research is partially supported by the National Key research and development program (2016YFC0106200), and 863 national research fund (2015AA043203) as well as the Chinese NSFC research fund (61190120, 61190124 and 61271318).

Compliance with ethical standards

Conflict of interest The authors declares that they have no conflict of interest.

Ethical standard No human participants were involved.

Informed consent Informed consent was obtained from all individual participants included in the study.

References

1. Nichols M, Townsend N, Scarborough P, Rayner M (2014) Cardiovascular disease in Europe 2014: epidemiological update. Eur Heart J 35:2950–2959. doi:10.1093/eurheartj/ehu299
2. Fu Y, Liu H, Huang W, Wang S, Liang Z (2009) Steerable catheters in minimally invasive vascular surgery. Int J Med Robot Comput Assist Surg 5:381–391. doi:10.1002/rcs.282
3. Aggarwal R, Black SA, Hance JR, Darzi A, Cheshire NJW (2006) Virtual reality simulation training can improve inexperienced surgeons' endovascular skills. Eur J Vasc Endovasc Surg 31:588–593. doi:10.1016/j.ejvs.2005.11.009
4. Neequaye SK, Aggarwal R, Van Herzeele I, Darzi A, Cheshire NJ (2007) Endovascular skills training and assessment. J Vasc Surg 46:1055–1064. doi:10.1016/j.jvs.2007.05.041
5. Ahmed K, Keeling AN, Fakhry M, Ashrafian H, Aggarwal R, Naughton PA, Darzi A, Cheshire N, Athanasiou T, Hamady M (2010) Role of virtual reality simulation in teaching and assessing technical skills in endovascular intervention. J Vasc Interv Radiol 21:55–66. doi:10.1016/j.jvir.2009.09.019
6. Dawson DL, Meyer J, Lee ES, Pevec WC (2007) Training with simulation improves residents' endovascular procedure skills. J Vasc Surg 45:149–154. doi:10.1016/j.jvs.2006.09.003
7. Lenoir J, Meseure P, Grisoni L, Chaillou C (2003) Surgical thread simulation. ESAIM Proc 12:102–107
8. Cotin S, Duriez C, Lenoir J, Neumann P, Dawson S (2005) New approaches to catheter navigation for interventional radiology simulation. Med Image Comput Comput Assist Interv 11:534–542
9. Lenoir J, Cotin S, Duriez C, Neumann P (2006) Interactive physically-based simulation of catheter and guidewire. Comput Graph 30:416–422. doi:10.1016/j.cag.2006.02.013
10. Dequidt J, Marchal M, Duriez C, Kerien E, Cotin S (2008) Interactive simulation of embolization coils: modeling and experimental validation. In: Lecture notes computer science (including subseries lecture notes artificial intelligence lecture notes in bioinformatics), vol 5241 LNCS, pp 695–702. doi:10.1007/978-3-540-85988-8_83
11. Alderliesten T, Bosman PAN, Niessen WJ (2007) Towards a real-time minimally-invasive vascular intervention simulation system. IEEE Trans Med Imaging 26:128–132. doi:10.1109/TMI.2006.886814
12. Spillmann J, Teschner M (2007) CORDE: Cosserat Rod Elements for the Dynamic Simulation of One-Dimensional Elastic Objects. Eurographics/ACM SIGGRAPH Symp Comput Animat 1:63–72. doi:10.2312/SCA/SCA07/063-072
13. Duratti L, Wang F, Samur E, Bleuler H (2008) A real-time simulator for interventional radiology. In: Proceedings of the 2008 ACM symposium on virtual reality software and technology—VRST '08, p 105. doi:10.1145/1450579.1450602
14. Basdogan C, Ho CH, Srinivasan MA (2001) Virtual environments for medical training: graphical and haptic simulation of laparoscopic common bile duct exploration. IEEE/ASME Trans Mechatron 6:269–285. doi:10.1109/3516.951365
15. Luboz V, Blazewski R, Gould D, Bello F (2009) Real-time guidewire simulation in complex vascular models. Vis Comput 25:827–834. doi:10.1007/s00371-009-0312-x
16. Tang W, Wan TR, Gould DA, How T, John NW (2012) A stable and real-time nonlinear elastic approach to simulating guidewire and catheter insertions based on cosserat rod. IEEE Trans Biomed Eng 59:2211–2218. doi:10.1109/TBME.2012.2199319
17. Bergou M, Wardetzky M, Robinson S, Audoly B, Grinspun E (2008) Discrete elastic rods. ACM Trans Graph 27:1. doi:10.1145/1360612.1360662
18. Tang W, Lagadec P, Gould D, Wan TR, Zhai J, How T (2010) A realistic elastic rod model for real-time simulation of minimally invasive vascular interventions. Vis Comput 26:1157–1165. doi:10.1007/s00371-010-0442-1
19. Luo M, Xie H, Xie L, Cai P, Gu L (2014) A robust and real-time vascular intervention simulation based on Kirchhoff elastic rod. Comput Med Imaging Graph 38:735–743. doi:10.1016/j.compmedimag.2014.08.002
20. Almeder C (1999) Hydrodynamic modelling and simulation of the human arterial blood flow. PhD thesis, Vienna University of Technology
21. Wu X, Allard J, Cotin S (2007) Real-time modeling of vascular flow for angiography simulation. Med Image Comput Comput Assist Interv 10:557–565
22. Zhu B, Iwata M, Haraguchi R, Ashihara T, Umetani N, Igarashi T, Nakazawa K (2011) Sketch-based dynamic illustration of fluid systems. ACM Trans Graph 30:1
23. Boisvert J, Poirier G, Borgeat L, Godin G (2013) Real-time blood circulation and bleeding model for surgical training. IEEE Trans Biomed Eng 60:1013–1022. doi:10.1109/TBME.2012.2230326
24. Pop SR, Hughes CJ, Ap Cenydd L, John NW (2013) A directed particle system for optimised visualization of blood flow in complex networks. Stud Health Technol Inform 184:330–336
25. Antiga L (2002) Patient-specific modeling of geometry and blood flow in large arteries. Politecnico di Milano
26. Luo Z, Cai J, Wang S, Zhao Q, Peters TM, Gu L (2013) Magnetic navigation for thoracic aortic stent-graft deployment using ultrasound image guidance. IEEE Trans Biomed Eng 60:862–871. doi:10.1109/TBME.2012.2206388